第37卷第5期
2018年10月

红外与毫米波学报
J. Infrared Millim. Waves

Vol. 37, No.5
October, 2018

文章编号: 1001-9014(2018)05-0513-06

DOI: 10.11972/j.issn.1001-9014.2018.05.001

High output power THz quantum cascade lasers and their temperature dependent performance

LIN Tsung-Tse*, WANG Ke, WANG Li, HIRAYAMA Hideki

(Center for Advanced Photonics, RIKEN 519-1399 Aramaki-aza Aoba, Aoba-ku, Sendai 980-0845, Japan)

Abstract: Quantum cascade lasers (QCLs) are promising high output power semiconductor-based terahertz (THz) sources with narrow linewidths and wide operating frequency. We have grown and fabricated THz-QCLs based on GaAs/AlGaAs superlattices under the guidance of a newly developed simulation tool based on the framework of Non-Equilibrium Green's Function (NEGF) method. The latest THz-QCLs demonstrated 270 mW peak power and 2.4 mW average power at 10 K, which is comparable to the highest reported value but with a size of more than 4 times larger than ours. Temperature dependence of the device performance are analyzed through the detailed calculations by using the NEGF method.

Key words: terahertz, quantum cascade lasers, GaAs

PACS: 42.55.Px; 85.30.De; 85.35.Be; 85.60.Bt

高输出功率太赫兹量子级联激光器与温度特性

林宗澤*，王 科，王 利，平山秀樹

(日本国立研究開発法人 理化学研究所 光量子工程研究领域 太赫兹量子器件研究室，仙台 980-0845，日本)

摘要: 半导体太赫兹量子级联激光器(THz QCL)是一种相干性好线宽窄的太赫兹辐射源，有潜力获得高的输出功率. 采用基于非平衡格林函数(NEGF)方法的计算工具设计、生长、制备了基于砷化镓系材料的THz QCL. 在10 K温度下，峰值功率达到270 mW，平均功率为2.4 mW，单位面积的输出功率与已报道的最高值相当. 采用NEGF方法对器件的温度变化特性做了详细的分析.

关 键 词: 太赫兹; 量子级联激光器; 砷化镓

中图分类号: O441　　**文献标识码:** A

Introduction

Terahertz (THz) quantum cascade lasers (QCLs)[1-2] are semiconductor-based compact coherent THz light sources, which employ carrier recycling and intersubband radiative transitions in periodically stacked quantum well structures. Such THz sources show narrow emission linewidth and have potential to deliver enough output power for real applications. The operating frequency range of THz-QCLs has been so far limited in the range from 1.2 to 5.2 THz[3-4]. The highest THz-QCL operating temperature of 199.5 K[5] was achieved for a state-of-art design with a metal-metal waveguide (MMW) and GaAs/AlGaAs active layers by using resonant tunneling injection and longitudinal optical (LO) phonon depopulation. However, the output power of THz-QCLs at such high temperatures is usually very low, which limits their applications. The diagonal emission designs for high temperature operation have the advantage to reduce leakage and to maintain better injection selectivity[5-7], but the diagonal transition leads to low output power. Consequently, low temperature operation is necessary and some cryogenic cooling systems must be used to obtain enough output power. Recently we have developed a compromise solution by using a liquid nitrogen (LN_2) Dewar condenser in order to maintain enough output power for real applications. The LN_2 Dewar condens-

Received date: 2017-12-07, **revised date:** 2018-04-26　　**收稿日期:** 2017-12-07, **修回日期:** 2018-04-26

Biography: LIN Tsung-Tse (1982-), male, Sendai, Japan, doctor. Research area involves THz and Mid-infrared quantum cascade lasers, fabrication of quantum structures by molecular beam epitaxy, and generally THz technology

* **Corresponding author:** E-mail: ttlin@riken.jp

?1994-2018 China Academic Journal Electronic Publishing House. All rights reserved. http://www.cnki.net

er is much smaller and less expensive than a liquid He based cryogenic system.

The output power is one of the most important parameters required for real THz applications. The research efforts include attempts to obtain large output power directly since the early state [8] and recent trials to control the far field pattern fabricated by cavity and antenna design with high output power [9-12]. The peak output power has been significantly increased since 2002, when the first THz-QCLs [2] were invented. The highest output power was reported to be 1 W peak power [13] at 10 K for a large size mesa and a semi-insulated surface plasmon waveguide (SI-SPW). However, the average output power is still much lower for THz-QCLs reported in a recent work [6]. Some recent reports have discussed the dynamic modeling [14], carrier transport properties [15], and temperature dependence of performance of THz QCLs [16].

In this work, we report high output power GaAs/AlGaAs THz-QCL based on resonant tunneling injection and longitudinal optical (LO) phonon depopulation scheme. Taking into account of the device size, we have obtained a record output power from our improved THz-QCL. The best THz-QCL mesa delivered 270 mW peak power at 10 K but only with a size of less than 1/4 of that for the highest reported 1 W THz QCL. The temperature dependence of this device is also analyzed and discussed.

1 Experiments

Here, the THz-QCL structure was grown by solid source Molecular Beam Epitaxy (MBE). The waveguides are SI-SPWs fabricated by a standard processing including photolithography and wet etching. Such SI-SPWs have better far field pattern. A typical mesa is with ridge width of 200 μm and cavity length of 2 mm. Previous MMW waveguide based THz QCLs can operated at high temperatures but the divergent far field pattern is one drawback for some applications [17-18]. The fabricated QCL mesas were loaded into a flowing liquid He cryostat and tested at various controlled temperature. The output power was measured by a well calibrated cryogenic Si-bolometer. The calibration was done by using a standard THz source with known output power, the is-TPG (injection-seeded THz-wave Parametric Generator), combined with commercial tip-up metalized Mylar film attenuators. The emission spectra were measured via a Fourier transform infrared spectrometer (FT-IR). Calculations of THz QCL transport and gain properties have been conducted in a framework of Non-Equilibrium Green´s Function (NEGF) method [19-24] by using the newly developed Nextnano. qcl tools from Nextnano Gmbh [25].

2 Results and discussion

We use the vertical emission design for the active region similar to the reported 4-wells structure [6]. The conduction band diagram under the operating bias of 45 mV per period and the corresponding wave functions are shown in Fig. 1. The active region includes 200 periods of $Al_{0.15}Ga_{0.85}As$/GaAs superlattices with barrier/well

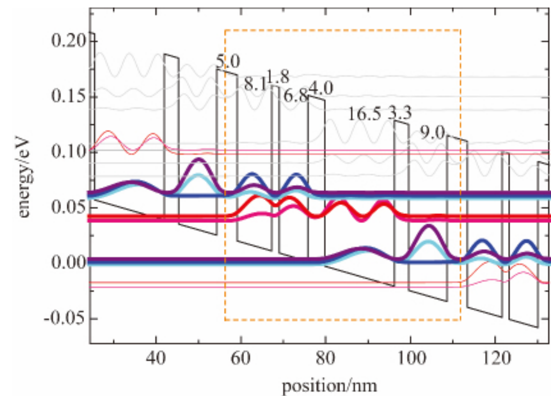

Fig. 1 Band diagram of high output power THz QCLs with barrier and well design of 5.0/8.1/1.8/6.8/4.0/16.5/3.3/9.0 (nm). The bias for one period is 45 mV

图 1 结构为 5.0/8.1/1.8/6.8/4.0/16.5/3.3/9.0 (nm) **的** THz QCL **的导带能带图,偏置电压为** 45 mV **每周期**

thicknesses of 5.0/8.1/1.8/6.8/4.0/16.5/3.3/9.0 (nm). In order to obtain high output power, vertical transition of the laser levels is adopted, with an oscillator strength of 0.89. The emission frequency of this QCL is around 4.25 THz, and the emission spectrum is shown in Fig. 2(a). The carriers are injected in pulse mode with a repetition rate of 1 k Hz and a duty cycle of 0.9%. Several longitudinal modes are clearly demonstrated in the spectrum. The measured (black solid line) and simulated (green line) current voltage curves are shown in Fig. 2(b). A maximum peak power of 270 mW has been obtained. This is a record power value if taking the device size into account. The reported highest power of 1.01 W was obtained in a QCL device with 425 um wide ridge, 4.2 mm long, and facet-coated mesa [13]. Here the device is only 0.2 × 2 mm, less than 1/4 of that in Ref 13. The threshold current density is at 315 A/cm^2, which is corresponding to a bias of 37 mV/period. This is indicated by the kinks in the J-V curves for both experimental and simulated results. The average power of 2.4 mW at 10 K has been obtained, as shown in Fig. 2(b). The measurement output power rapidly decreases above 100 K and the maximum operation temperature of fabricated device is 125 K as shown in Fig. 2(b).

This design enables the resonant tunneling injection process, and the LO phonon depopulation process, with enhanced vertical transition. After the injection well (9.0 nm) and two emission wells (8.2 nm and 6.8 nm), the widest extraction well (16.4 nm) is used for LO phonon scattering depopulation. Such a design can give large oscillator strength between upper and lower lasing levels, which is beneficial for obtaining relatively larger output power at low temperatures, and more smooth injection. But the large oscillator strength can also increase the probability of thermal back filling [26-28], which reduce the population inversion due to increased thermal energy at higher temperature [29-32].

At elevated temperature, 80 K, this device delivered only 10 mW peak power and 0.09 mW average power, much reduced compared to at 10 K. Such a value is

?1994-2018 China Academic Journal Electronic Publishing House. All rights reserved. http://www.cnki.net

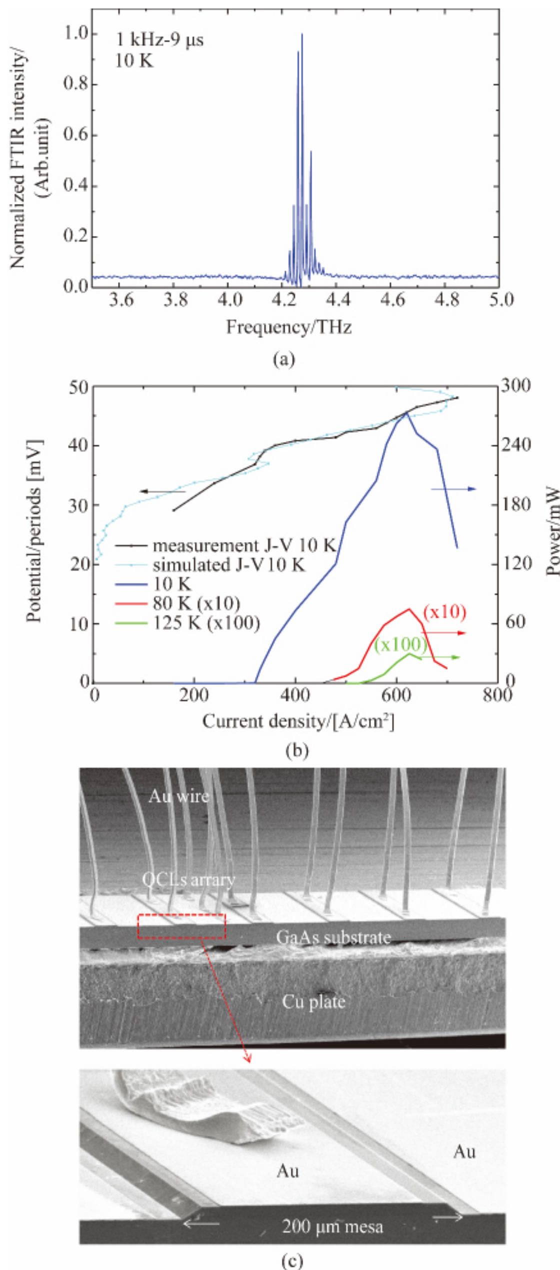

Fig. 2　(a) Lasing spectrum of THz QCLs with maximum output power at 45 mV per period; (b) Current - voltage characteristics and current density - light output characteristics at 10 K. The black line is the measured J-V curves, and the green line is the calculated one; (c) SEM microscopy of fabricated THz QCL devices

图 2　(a) 工作电压时,45 mV 每周期,的 THz QCL 的激光光谱,(b) 10 K 温度时的电流-电压及电流-光输出特性曲线. 黑线为测得结果,浅蓝线为计算结果,(c) 器件的 SEM 图

only slightly improved compared to our previous results. The simulated energy and position resolved carrier densities at 10 K, 80 K, and 150 K are shown in Fig. 3 respectively. The red dashed squares indicate one period. The wavefunctions of the Wannier-Stark levels are plotted in white lines. Figure 4 (a) shows the calculated optical gain mapping as functions of applied bias from 30 to 70 mV per period (X axis) and temperature from 5 to 220 K (Y axis). Figure 4 (b) are the calculated gain as functions of applied bias at three typical temperatures, namely, 10 K, 80 K, and 150 K, which are corresponding to the three dashed lines in Fig. 4 (a).

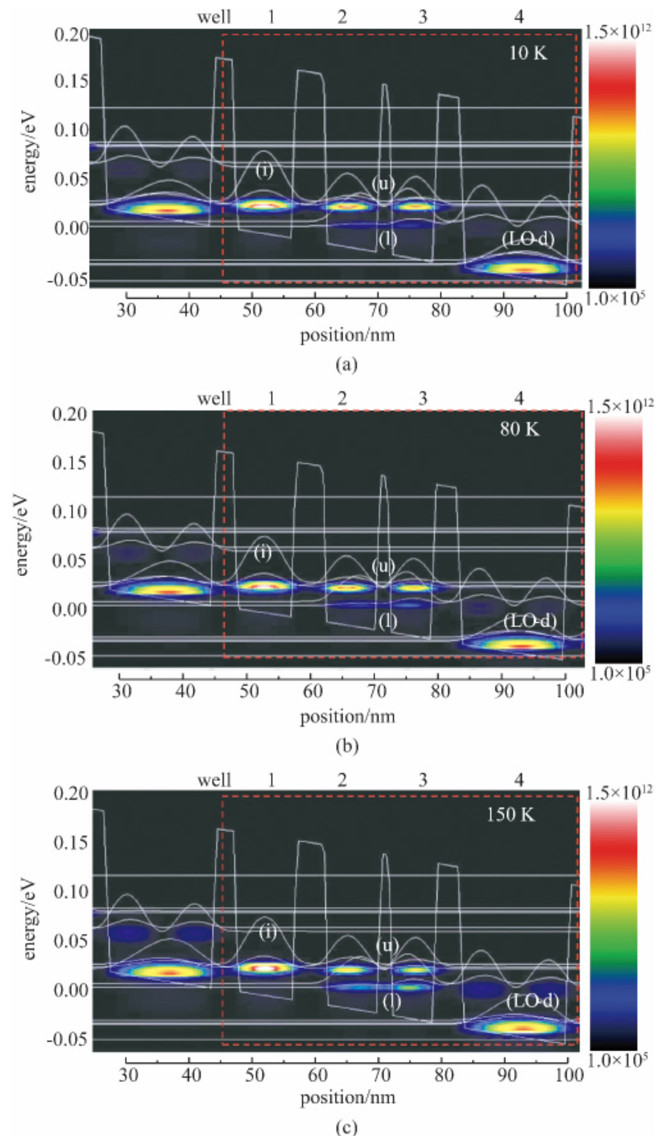

Fig. 3　Calculated carrier density and wave functions of the Wannier-Stark levels by NEGF method at (a) 10 K (b) 80 K (c) 150 K. (i) indicate injection level, (u) indicate upper lasing level, (l) indicate lower lasing level, and (LO-d) indicate LO depopulation level

图 3　采用 NEGF 法计算所得不同温度下的电子浓度位置-能量分布和 Wannier-Stark 态的波函数. (a) 10 K,(b) 80 K,(c) 150 K. (i) 为注入态,(u) 为激光上能级,(l) 为激光下能级,(LO-d) 为声子抽取基态

As can be seen in Fig. 3 (a), at 10 K, the carrier density distribution spots have clearly demonstrated population inversion between the upper and lower lasing levels, marked as (u) and (l). The peak carrier density of the upper lasing level is 1.5×10^{12} $cm^{-3}eV^{-1}$, which is significantly higher than that of the lower lasing level, $\sim1\times10^{8}$ $cm^{-3}eV^{-1}$. At the same time, the overlap of

?1994-2018 China Academic Journal Electronic Publishing House. All rights reserved.　http://www.cnki.net

these two wavefunctions are high, indicating the vertical transition nature in the emission wells 2 and 3. The injector level in the well 1 is aligned with the upper lasing level. The lower lasing level is aligned with the extraction level in the well 4, where the carrier spots are weak but can be identified and become clearer in Fig. 3 (b, c). The carriers are then depopulated by the fast LO phonon scattering in the well 4 and then injected into the next period. The calculated peak gain is 193 cm^{-1}, a large value, as shown in Fig. 4. Compared to the typical SI-SPW facet/mirror and waveguide loss of ~40 cm^{-1}, the large gain is consistent with the measured large output power.

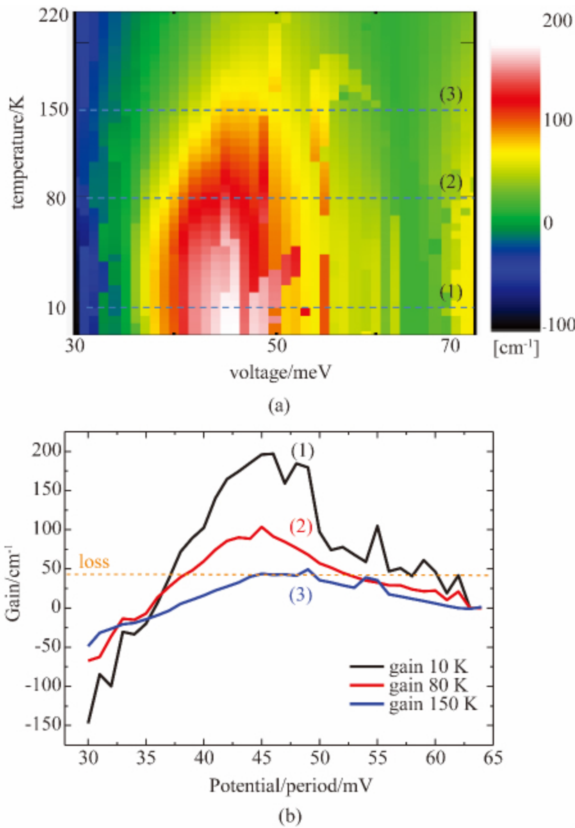

Fig. 4 (a) Calculated gain mapping by NEGF method. Plotted the active region net gain with operation temperature and external electric field. (b) Three calculated gain spectra as functions of applied bias indicated by the dashed lines in (a)

图 4 采用 NEGF 法计算所得增益的电压-温度变化图. (b) 计算所得三个温度下,工作电压时的增益谱

As the temperature increases, we can see the carrier density in the lower lasing level increases obviously, as shown in Fig. 3 (b, c). The required population inversion to overcome the loss is still satisfied at 80 K. The peak carrier density of the upper and lower lasing level is 1.3×10^{12} $cm^{-3}eV^{-1}$ and ~5×10^{8} $cm^{-3}eV^{-1}$, respectively. The calculated peak gain is near 100 cm^{-1} at 80 K, corresponding to the measured 10 mW peak power. However, as the temperature increases further up to 150 K, although the population inversion is still kept, the gain is much reduced to the level around the total loss. As indicated in Fig. 3 (c), peak carrier density at upper lasing level is only 7.4×10^{11} $cm^{-3}eV^{-1}$. More striking, the occupation of the lower level increases obviously to an unacceptable level, ~2×10^{11} cm^{-3} eV^{-1}. The peak gain reduces to only about 45 cm^{-1}, just around the estimated total loss. Consequently, lasing would be difficult to achieve.

The actual maximum operation temperature of this device is lower than the calculated 150 K. This is attributed to the underestimated electron-electron (e-e) interactions in the calculation model. In this calculation, the e-e interaction is approximated as an averaged potential accounted in Poisson's equation by using the Hartree term only. Consequently, the e-e scattering is underestimated and the gain is thus overestimated. We are trying to include the high order terms beyond the Hartree term in the NEGF simulation, and the preliminary results indicate that the absolute gain values are overestimated by about 30% at around 120-150 K for this particular design. Further work is ongoing to improve the absolute values closer to real situations. Nevertheless, the qualitative trend of temperature dependence remains similar as shown in Fig. 4 and explains the experimental results.

There are three physical processes attributed to the reduction of population inversion and thus the gain at elevated temperatures. First, the thermal energy excited phonon scattering induced depopulation from the upper lasing level to the lower one, as the carriers obtain enough thermal energy at high temperatures. This is more severe in vertical transition design. Second, thermal backfilling by absorption of LO phonons and filling back to the lower lasing levels. These two processes have been the well known origins accounting the operation temperature limitation, so far ~200 K. However, for this particular design, the gain reduces with increasing temperature is actually faster than expectation. Besides the above

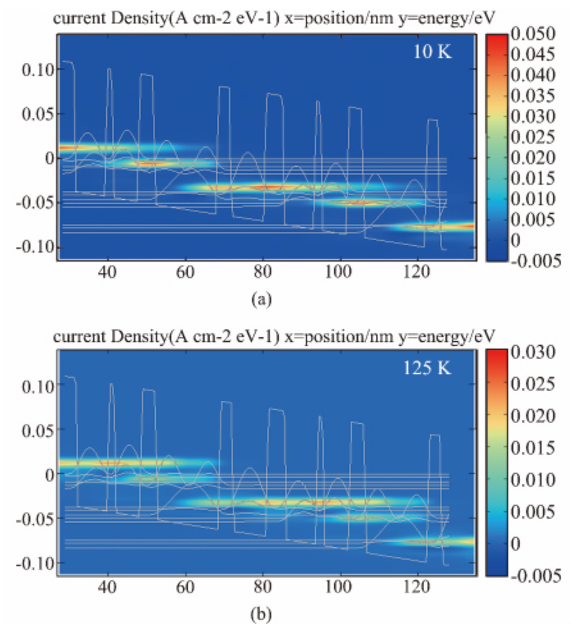

Fig. 5 Calculated energy and space resolved current density at a bias of 44 meV/period at (a) 10 K and (b) 125 K

图 5 计算所得工作电压时的能量-位置解析的电流密度分布. (a) 10 K,(b) 125 K

?1994-2018 China Academic Journal Electronic Publishing House. All rights reserved. http://www.cnki.net

two reasons, the current density mapping at 10 K and 125 K in Fig. 5 also demonstrate a current leakage channel direct from the upper lasing level to the extraction level through the extraction barrier into the widest well (16.5 nm). This leakage current is significantly larger at 125 K, clearly seen in Fig. 5 (b), contrasting to 10 K. Therefore, extra depopulation through this leakage channel is activated as temperature increases, leading to much reduced gain. Thicker extraction barrier would reduce such leakage, but at the same time would reduce the extraction efficiency. We are now redesigning the structure with the guidance of the NEGF method based simulations to improve the performance.

3 Conclusions

In this work, we have grown and fabricated a high output power THz-QCL and discussed the temperature dependence of its performance. Taking the device size into account, we have obtained a record output peak power, which is 270 mW at 10 K but with a size of less than 1/4 of the THz QCL previously reported to deliver the highest power. The gain calculations by NEGF methods have demonstrated clear improved performance for the more vertical transition design at low temperature, which is consistent with the experimental results. But at higher temperatures, the population inversion reduces significantly due to the thermal backfilling and thermally activated LO phonon depopulation of the upper lasing level. Further optimization of the THz QCLs is ongoing to improve their performance at around LN_2 temperature, for the purpose of integrating the THz-QCLs into a home-made 77 K LN_2 Dewar condenser, which is relatively compact and can deliver a few tens of mW peak power and sub-mW average power for some real THz imaging applications.

Acknowledgments

The Non-Equilibrium Green's Function (NEGF) method calculations in this work has been conducted by using nextnano. QCL simulation tool developed by Nextnano GmbH.

Explanation to the innovation

In this manuscript, we have grown and fabricated THz QCLs based on GaAs/AlGaAs superlattices with the guidance of a newly developed simulation tool within the framework of Non-Equilibrium Green's Function (NEGF) method. The latest THz-QCLs have demonstrated 270 mW peak power and 2.4 mW average power at 10 K, which is comparable to the highest ever report THz QCL with 1 W output power but with a size of more than 4 times larger than our devices. But at 80 K, the output peak power reduces to 10 mW rapidly. Temperature dependence of the device performance are analyzed based on the detailed calculations by the NEGF method.

References

[1] Faist J, Capasso F, Sivco D L, *et al*. Quantum cascade laser [J]. *Science*, 1994, 264: 553-556.

[2] Köhler R, Tredicucci A, Beltram F, *et al*. Terahertz semiconductor-heterostructure laser [J]. *Nature*, 2002, **417**: 156-159.

[3] Walther C, Fischer M, Scalari G, *et al*. Quantum cascade lasers operating from 1.2 to 1.6THz [J]. *Appl. Phys. Lett.*, 2007, **91**: 131122-1-131122-3.

[4] Chan C W I, Hu Q, Reno J L, Ground state terahertz quantum cascade lasers [J]. *Appl. Phys. Lett.* 2012, **101**: 151108-1-151108-4.

[5] Fathololoumi S, Dupont E, Chan C W I, *et al*. Terahertz quantum cascade lasers operating up to ? 200 K with optimized oscillator strength and improved injection tunneling [J]. *Opt. Express*, 2012, **20**: 3866-3876.

[6] Albo A, Hu Q. Carrier leakage into the continuum in diagonal GaAs/$Al_{0.15}$GaAs terahertz quantum cascade lasers [J]. *Appl. Phys. Lett.*, 2015, **107**: 241101-1-241101-5.

[7] Kumar S, Chan C W I, Hu Q, *et al*. Two-well terahertz quantum-cascade laser with direct intrawell-phonon depopulation [J]. *Appl. Phys. Lett.*, 2009, **95**: 141110-1-141110-3.

[8] Williams B S, Kumar S, Hu Q, *et al*. High-power terahertz quantum-cascade lasers [J]. *Electron. Lett.*, 2006, **42**: 89-90.

[9] Lee A W M, Qin Q, Kumar S, *et al*. High-power and high-temperature THz quantum-cascade lasers based on lens-coupled metal - metal waveguides [J]. *Opt. Lett.*, 2007, **32**: 2840-2842.

[10] Mendis R, Nagai M, Wang Y, *et al*. Terahertz Artificial Dielectric Lens [J]. *Sci. Rep.*, 2016, **6**: 1-8.

[11] Zhu H, Wang F, Yan Q, *et al*. Terahertz master-oscillator power-amplifier quantum cascade lasers [J]. Appl. Phys. Lett., 2016, **109**: 231105-1-231105-5.

[12] Ohtani K, Turcinkova D, Bonzon C, *et al*. High performance 4.7 THz GaAs quantum cascade lasers based on four quantum wells [J]. *New. J. Phys.*, 2016, **18**: 123004.

[13] Li L, Chen L, Zhu J, *et al*. Terahertz quantum cascade lasers with > 1 W output powers [J]. *Eectron. Lett.* 2014, **50**: 309-311.

[14] Hamadou A, Thobel J-L, Lamari S. Dynamic modeling of optically pumped electrically driven terahertz quantum cascade lasers [J]. *Infrared phys. technol.*, 2017, **81**: 195-200.

[15] Li L, Zhou X H, Lin T, *et al*. Electronic transport in a long wavelength infrared quantum cascade detector under dark condition [J]. *Infrared phys. technol.*, 2016, **78**: 72-75.

[16] Saha S, Kumar J. Complete rate equation modelling of quantum cascade lasers for the analysis of temperature effects [J]. *Infrared phys. technol.* 2016, **79**: 85-90.

[17] Maineult W, Gellie P, Andronico A, *et al*. Metal-metal terahertz quantum cascade laser with micro-transverseelectromagnetic-electromagnetic-horn antenna [J]. *Appl. Phys. Lett.* 2008, **93**: 183508-1-183508-3.

[18] Orlova E E, Hovenier J N, Klaassen T O, *et al*. Antenna Model for Wire Lasers [J]. *Phys. Rev. Lett.*, 2006, **96**: 173904.

[19] Yasuda H, Kubis T, Vogl P, *et al*. Nonequilibrium Green's function calculation for four-level scheme terahertz quantum cascade lasers [J]. *Appl. Phys. Lett.* 2009, **94**: 151109-1-151109-3.

[20] Schmielau T, Pereira Jr M F. Nonequilibrium many body theory for quantum transport in terahertz quantum cascade lasers [J]. *Appl. Phys. Lett.*, 2009, **95**: 231111-1-231111-3.

[21] Wacker A, Lindskog M, Winge D O. Nonequilibrium Green's Function Model for Simulation of Quantum Cascade Laser Devices Under Operating Conditions [J]. *IEEE J. Sel. Top. Quant. Electron*, 2013, **19**: 1200611.

[22] Jirauschek C, Kubis T, Modeling techniques for quantum cascade lasers [J]. *Appl. Phys. Rev.*, 2014, **1**: 011307-1-011307-51.

[23] Grange T, Contrasting influence of charged impurities on transport and gain in terahertz quantum cascade lasers [J]. *Phys. Rev. B*, 2015, **92**: 241306.

[24] Winge D O, Franckie M, Verdozzi C, *et al*. Simple electron-electron scattering in non-equilibrium Green's function simulations [J]. *J. Phys. Conf. Series*, 2016, **696**: 012013.

[25] Nextnano Gmbh, http://www.nextnano.de/

(下接第 522 页)

?1994-2018 China Academic Journal Electronic Publishing House. All rights reserved. http://www.cnki.net

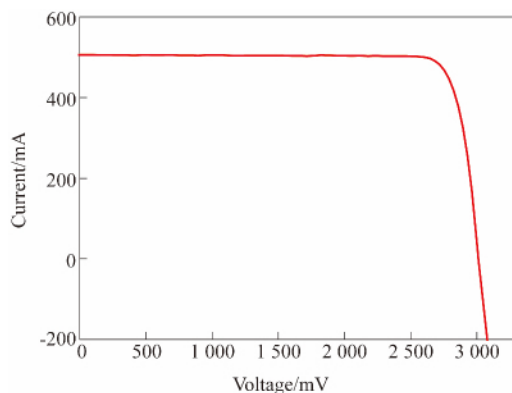

Fig. 7 Photovoltaic *I-V* characteristics of flexible InGaP/GaAs/InGaAs solar cell

图 7 柔性 InGaP/GaAs/InGaAs **太阳电池的光照** *I-V* **曲线**

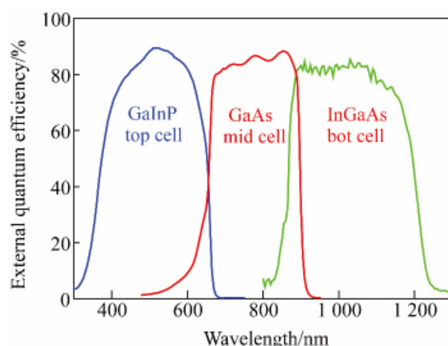

Fig. 8 External quantum efficiency of flexible InGaP/GaAs/InGaAs solar cell

图 8 柔性 InGaP/GaAs/InGaAs **太阳电池的外量子效率**

GaAs epitaxial layers have been fabricated. Combined with flexible thin film solar cells preparation process, 30 cm^2 large area flexible GaInP/GaAs/InGaAs 3-junciton solar cells on 50 μm polyimide film achieved a 1-sun, AM0 conversion efficiency of 31.5% with an open-circuit-voltage of 3.01 V, a short-circuit current-density of 16.8 mA/cm^2, and a fill factor of 0.845. By using the very light PI substrate, the unit weight of the solar cell is only 168.5 g/m^2 and the specific power is up to 2 530 W/kg.

References

[1] Sato S I, Miyamoto H, Imaizumi M, *et al.* Degradation modeling of InGaP/GaAs/Ge triple-junction solar cells irradiated with various-energy protons [J]. *Solar Energy Materials & Solar Cells*, 2009, **93**(6): 768-773.

[2] Lan D, Green M A. Limiting efficiencies of GaInP/GaAs/Ge up-conversion systems: Addressing the issue of radiative coupling [J]. *Applied Physics Letters*, 2016, **109**(12): 42.

[3] Geisz J F, Kurtz S, Wanlass M W, *et al.* High-Efficiency GaInP/GaAs/InGaAs Triple-Junction Solar Cells Grown Inverted with a Metamorphic Bottom Junction [J]. *Applied Physics Letters*, 2007, **91**(2): 760.

[4] Yablonovitch E, Gmitter T, Harbison J P, *et al.* Extreme selectivity in the lift - off of epitaxial GaAs films [J]. *Applied Physics Letters*, 1987, **51**(26): 2222-2224.

[5] Cheng C W, Shiu K T, Li N, *et al.* Epitaxial lift-off process for gallium arsenide substrate reuse and flexible electronics [J]. *Nat Commun*, 2013, **4**: 1577.

[6] Schermer J J, Mulder P, Bauhuis G J, *et al.* Epitaxial Lift-Off for large area thin film III/V devices [J]. *physica status solidi (a)*, 2005, **202**(4): 501-508.

[7] Wu F-L, Ou S-L, Horng R-H, *et al.* Improvement in separation rate of epitaxial lift-off by hydrophilic solvent for GaAs solar cell applications [J]. *Solar Energy Materials and Solar Cells*, 2014, **122**: 233-240.

[8] Moon S, Kim K, Kim Y, *et al.* Highly efficient single-junction GaAs thin-film solar cell on flexible substrate [J]. *Sci Rep*, 2016, **6**: 30107.

[9] Nam J, Lee Y, Choi W, *et al.* Transfer Printed Flexible and Stretchable Thin Film Solar Cells Using a Water-Soluble Sacrificial Layer [J]. *Advanced Energy Materials*, 2016, **6**(21): 1601269.

[10] Ward J S, Remo T, Horowitz K, *et al.* Techno-economic analysis of three different substrate removal and reuse strategies for III-V solar cells [J]. *Progress in Photovoltaics: Research and Applications*, 2016, **24**(9): 1284-1292.

[11] Johnson D C, Ballard I, Barnham K W J, *et al.* Advances in Bragg stack quantum well solar cells [J]. *Solar Energy Materials & Solar Cells*, 2005, **87**(1): 169-179.

(上接第 517 页)

[26] Lin T-T, Ohtani K, Ohno H. Thermally Activated Longitudinal Optical Phonon Scattering of a 3.8 THz GaAs Quantum Cascade Laser [J]. *Appl. Phys. Express*, 2009, **2**: 022102-1-022102-3.

[27] Matyas A, Chashmahcharagh R, Kovacs I, *et al.* Improved terahertz quantum cascade laser with variable height barriers [J]. J. Appl. Phys. 2012, **111**: 103106-1-103106-6.

[28] Lin T-T, Hirayama H. Variable Barrier Height AlGaAs/GaAs Quantum Cascade Laser Operating at 3.7 THz [J]. *Phys. Status Solidi A*, 2018, **215**: 1700424.

[29] Lin T-T, Ying L, Hirayama H. Threshold Current Density Reduction by Utilizing High-Al-Composition Barriers in 3.7 THz GaAs/$Al_xGa_{1-x}As$ Quantum Cascade Lasers [J]. *Appl. Phys. Express*, 2011, **5**: 012101-1-012101-3.

[30] Luo H, Laframboise S R, Wasilewski Z R, *et al.* Terahertz quantum-cascade lasers based on a three-well active module [J]. *Appl. Phys. Lett.* 2007, **90**: 041112-1-041112-3.

[31] Kumar S, Hu Q, Reno J R, 186 K operation of terahertz quantum-cascade lasers based on a diagonal design [J]. *Appl. Phys. Lett.* 2009, 94: 131105-1-131105-3.

[32] Lin T-T, Hirayama H. Improvement of operation temperature in GaAs/AlGaAs THz - QCLs by utilizing high Al composition barrier [J]. *Phys. Status Solidi C*, 2013, **10**: 1430-1433.

?1994-2018 China Academic Journal Electronic Publishing House. All rights reserved. http://www.cnki.net